Micro-scale visualization of Microbial-Induced Calcium Carbonate Precipitation (MICP) processes

Yuze Wang[1]; Kenichi Soga[2]; Jason T. DeJong[3]; Alexandre J. Kabla[4]

[1]*Department of Engineering, University of Cambridge, Cambridge, UK. ORCID: 0000-0003-3085-5299. E-mail: yw369@cam.ac.uk*

[2]*Department of Civil and Environmental Engineering, University of California, Berkeley, CA 94720, United States. E-mail: soga@berkeley.edu*

[3]*Department of Civil and Environmental Engineering, University of California, Davis, CA 95616, United States. Email: jdejong@ucdavis.edu*

[4]*Department of Engineering, University of Cambridge, Cambridge, UK. ORCID: 0000-0002-0280-3531. Email: ajk61@cam.ac.uk*

Abstract: Microbial-Induced Calcium Carbonate ($CaCO_3$) Precipitation (MICP) has been explored for its potential engineering applications such as soil stabilization, but our understanding of the fundamental MICP processes at the microscale is limited. In this study, real-time *in situ* micro-scale experiments were conducted using glass slides and microfluidic chips (synthetic porous media which simulate soil matrices to model the conditions similar to actual MICP treatments) to visualize the $CaCO_3$ precipitation process. The results of this study show that irregularly-shaped $CaCO_3$ precipitates initially emerged on bacterial aggregates and subsequently dissolved with time as regularly-shaped $CaCO_3$ crystals started growing; less stable and smaller $CaCO_3$ crystals may dissolve at the expense of growth of more stable and larger $CaCO_3$ crystals. The time-dependent phase transformation of $CaCO_3$ precipitates makes the size of the crystals formed during MICP highly dependent on the time interval between cementation solution injections during a staged injection procedure. When the injection interval was 3-5 hours, a larger number of crystals (200-1000 per 10^6 μm^3) with smaller sizes (5-10 μm) was produced. When the

injection interval was longer (23-25 hours), the crystals were larger (10-80 μm) and fewer in number (5-20 per 10^6 μm^3). The direct observation of MICP processes in this study improves the understanding of MICP fundamentals and the effect of MICP processes on the properties of $CaCO_3$ crystals formed after MICP treatment. These observations will therefore be useful for designing future MICP treatment protocols which improve the properties and sustainability of MICP-treated samples.

INTRODUCTION

Microbial-Induced Calcium Carbonate Precipitation (MICP) is a bio-geochemical process in which microbial activity alters the surrounding aqueous environment and induces calcium carbonate ($CaCO_3$) precipitation (Stocks-Fischer et al. 1999; DeJong et al. 2006). Due to its ease of control, high chemical conversion efficiency and rapid operation process (Dhami et al. 2013), MICP occurring via a urea-hydrolysis pathway has been extensively studied for its potential subsurface applications such as soil stabilization (Whiffin et al. 2007; DeJong et al. 2006, 2010; van Paassen et al. 2010; Al Qabany and Soga 2013), erosion control (Jiang et al. 2017) and hydraulic control (Phillips et al. 2013). During the ureolysis-driven MICP process, bacteria with ureolytic activity express intracellular urea amidohydrolase, a urease enzyme which catalyzes the hydrolysis of urea (equation 1); the addition of calcium (Ca^{2+}) to this system induces the precipitation of calcium carbonate ($CaCO_3$) as the resulting CO_3^{2-} ions react with the supplied Ca^{2+} cations (equation 2):

$$CO(NH_2)_2 + 2H_2O \xrightarrow{Urease} 2NH_4^+ + CO_3^{2-} \quad (1)$$

$$Ca^{2+} + CO_3^{2-} \rightarrow CaCO_3(s) \quad (2)$$

Research has shown that the $CaCO_3$ crystals can bond soil particles together, which strengthens the soil (DeJong et al. 2006, 2010) and can also fill the pores of the soil matrix, thus reducing soil permeability (Al Qabany and Soga 2013). This improvement in soil strength and permeability is not only dependent on the macro-scale $CaCO_3$ content (the mass of $CaCO_3$ precipitates divided by the total mass of $CaCO_3$ precipitates and soil particles, defined by Whiffin et al. 2007, van Paassen et al. 2010, and Al Qabany and Soga 2013) but is also highly dependent on the micro-scale properties of $CaCO_3$ precipitates (DeJong et al. 2010; Al Qabany and Soga 2013; Lin et al. 2016; Wang et al. 2017). Previous MICP studies have shown a large variation in the micro-scale properties of $CaCO_3$ crystals such as size and shape (van Paassen et al. 2010; Al Qabany and Soga 2013). However, the reasons for the formation of different sizes and shapes of $CaCO_3$ precipitates remain poorly understood.

$CaCO_3$ precipitates have a number of polymorphs such as rhombohedral calcite (Kawano et al. 2002; Lian et al. 2006; Dhami et al. 2013), spherical vaterite (Kawano et al. 2002; Lian et al. 2006; van Paassen 2009; Dhami et al. 2013), aragonite which normally crystallizes as clustered needles (Morse et al. 2007; Dhami et al. 2013) at high temperature (higher than 35 °C, Ogino et al. 1987; Carteret et al. 2009), and non-crystalline amorphous calcium carbonate (ACC) nano-particles which have a complex hybrid structure (Kawano et al. 2002; Bots et al. 2012; Dhami et al. 2013; Rodriguez-Blancoet al. 2011). Four images showing the $CaCO_3$ polymorphs reported in the literature are summarized in Figure 1. These $CaCO_3$ polymorphs not only vary in their morphology, but also vary in their stability and precipitation rate. Usually, the least stable phase forms first and transforms into the next stable phase until finally, the most stable phase forms (reviewed by Cöelfen and Antonietti, 2008). The phase transformation during precipitation

processes is consistent with Ostwald's step rule (Cöelfen and Antonietti, 2008) and has been observed during $CaCO_3$ precipitation in previous studies. Wei et al. (2003) observed the transformation from vaterite to calcite. Kawano et al. (2002) and Rodriguez-Blanco et al. (2011) reported that ACC forms first and subsequently transforms to calcite via the intermediate formation of vaterite. With the phase transformation of $CaCO_3$ precipitates, the shape and size of the $CaCO_3$ precipitates change accordingly (Kawano et al. 2002; Bots et al. 2012). The phase transformations of $CaCO_3$ reported previously were based on the chemical precipitation of $CaCO_3$ induced by $CaCl_2$ and Na_2CO_3, rather than on the precipitation of $CaCO_3$ induced by bacteria. However, the similarities and differences between these two processes are as yet largely unknown. Furthermore, the shapes, sizes and stabilities of $CaCO_3$ precipitates are very important factors that affect the engineering properties of MICP-treated soils (van Paassen 2009; DeJong et al. 2010; Al Qabany and Soga 2013; Lin et al. 2016; Wang et al. 2017). Therefore, a better understanding of (i) the phase transformation of $CaCO_3$ during MICP and (ii) the changes in shape and size of $CaCO_3$ precipitates with time will be helpful for designing MICP treatment protocols that improve the engineering properties of MICP-treated samples.

A widely-held assumption of the $CaCO_3$ precipitation process during MICP is that bacterial cells serve as $CaCO_3$ nucleation sites and that once the nucleation sites form, the $CaCO_3$ crystals continue growing from them (Stocks-Fischer et al. 1999; Hammes et al. 2002; DeJong et al. 2006; Dhami et al. 2013; Ganendra et al. 2014). This is assumed because bacterial cell walls are negatively charged and can adsorb Ca^{2+} (EI Mountassir et al. 2014). Therefore, once the bacterial cells hydrolyze the urea, the released CO_3^{2-} ions precipitate with the Ca^{2+} cations which are attached to the bacterial cell walls, forming the $CaCO_3$ nucleation required for $CaCO_3$ crystal growth.

However, this assumption has been questioned by the observation that $CaCO_3$ can precipitate in the absence of bacterial cells (Mitchell and Ferris, 2006) and that some of the bacterial cells in the mixture of the bacterial suspension and the urea-$CaCl_2$ solution did not have $CaCO_3$ precipitates formed on them by 20 hours after mixing (van Paassen 2009). In addition, $CaCl_2$ can cause the formation of bacterial aggregates which induce $CaCO_3$ precipitation (El Mountassir et al. 2014). However, because the microscope and digital camera used in these studies were not able to capture images at the bacterial size level, neither the effects of individual bacterial cells on the $CaCO_3$ nucleation and growth, nor the effects of bacterial aggregates on $CaCO_3$ precipitation are fully understood.

In this study, we conducted *in situ* micro-scale experiments with the following aims: (i) to observe the evolution of the shape and size of the $CaCO_3$ precipitates during the MICP process, (ii) to understand the effects of bacterial cells/aggregates on $CaCO_3$ precipitation, and (iii) to vary the treatment procedure in an attempt to establish a correlation between the $CaCO_3$ precipitation process and the final size of $CaCO_3$ crystals. Micro-scale experiments were conducted using glass slides and microfluidic chips to simulate non-porous media and porous media where MICP processes occur. A high resolution optical microscope capable of observing both bacterial cells and $CaCO_3$ precipitates in either glass slides or microfluidic chips was utilized. In the glass slide experiments, the MICP process after mixing bacterial suspension with cementation solution was captured to explore the evolution of the shape and size of the $CaCO_3$ precipitates and the effects of bacterial cells/aggregates on $CaCO_3$ precipitation. In the microfluidic chip experiments, microfluidic chips containing flow injection channels and synthetic porous media were used to observe the $CaCO_3$ precipitation process during staged-injection MICP procedures. These

experiments involved a single injection of bacterial suspension followed by either one, two or twelve injections of cementation solution with a time interval of either 3-5 hours or 23-25 hours between injections. Three microfluidic chip experiments were conducted to explore: (1) whether bacterial aggregation occurs during successive injections of bacterial suspension and cementation solution; (2) whether $CaCO_3$ precipitation occurs after the first and the second injections of cementation solution in the same way as observed in the glass slide experiment; and (3) whether different MICP treatment procedures produce $CaCO_3$ crystals with different sizes when the injection interval between two successive injections of cementation solution is varied. The practical implications of these findings are also discussed.

MATERIALS AND METHODS

Bacterial suspension

Sporosarcina pasteurii (*S. pasteurii*, strain DSM 33, purchased from DSMZ, Germany) was used in the experiments described in this study. *S. pasteurii* is a naturally occurring strain of soil bacteria which has high ureolysis activity (Whiffin 2007). *S. pasteurii* bacterial suspension was prepared using a freeze-dried *S. pasteurii* stock, which was activated according to the manufacturer's guidelines (DSMZ). After activation, glycerol stocks of the bacteria were prepared by adding 225 μl of 80% glycerol (autoclaved) to 1 ml of overnight liquid culture in cryogenic vials, after which the liquid culture was immediately frozen at -80°C. Once defrosted, cells from the glycerol stock were grown in American Type Culture Collection (ATCC) 1376 NH_4-YE agar medium (20 g/L yeast extract, 10 g/L ammonium sulphate, 20 g/L agar and 0.13 M Tris base) for 48 hours at 30°C. Subsequently, several colonies on the agar plate were picked and transferred to a NH_4-YE liquid medium containing the same components as ATCC 1376 NH_4-YE but without

agar, and cultivated in a shaking incubator for 24 hours at 30°C and a shaking rate of 200 rpm to obtain a bacterial suspension with an optical density measured at a wave length of 600 nm (OD_{600}) of around 3.0. Because the type of enzyme produced by *S. pasteurii* is intracellular, there is no release of urease from the bacterial cells during cultivation. The bacterial suspension with lower OD_{600} was obtained by diluting this bacterial suspension using NH_4-YE liquid medium.

Cementation solution

The cementation solution for MICP treatment was created using calcium chloride dihydrate ($CaCl_2 \cdot 2H_2O$), urea ($CO(NH_2)_2$), and Thermo Scientific™ Oxoid™ Nutrient Broth dissolved in deionized water. Two concentrations of calcium chloride were used: 0.25 M and 1.0 M. The concentration of urea was 1.5 times higher than that of calcium chloride, and the concentration of nutrient broth was constant at 3 g/L. All chemicals used were of analytical reagent grade.

Glass slide experiment

Experiments on glass slides were conducted to examine the evolution of the shape and size of $CaCO_3$ precipitates in the mixture of bacterial suspension and cementation solution with time (Figure 2). Glass slide samples were prepared by placing two successive 5 μl drops of bacterial suspension and cementation solution at the center of an optically transparent glass slide, after which an optically transparent cover slip was placed on top of the liquid specimen. Subsequently, the edges of the cover slips were sealed using nail varnish to avoid the drying of the liquid specimen on the glass slides (van Paassen 2009). The reported optical densities of bacterial suspension and concentration of cementation solution used during MICP treatment in the literature are in the range of 0.2-2.5 and 0.1-1.5 M, respectively (Al Qabany et al. 2012; Jiang et al. 2017;

Cheng et al. 2017). The optical densities of bacterial suspension and the concentrations of cementation solution used in this study were within the range of the bacterial densities and concentrations of cementation solution reported in the literature and are shown in Table 1. Test 1 was conducted to observe bacterial behavior after the bacterial suspension was mixed with cementation solution or with each of the individual components of the cementation solution. Test 2 was conducted to examine the evolution of the shape and size of $CaCO_3$ precipitates in the mixture of bacterial suspension and cementation solution with time. Time series images of the sample in Test 2 were continuously captured at an imaging interval of five minutes over a time period of twelve hours. The time '0 minutes' or '0 hours' was the time when the first image of the sample was taken, which was about two minutes after mixing of bacterial suspension with cementation solution.

Microfluidic chip experiments

A staged injection procedure has been widely applied during MICP treatment for improving the strength and stability of soils (DeJong et al. 2006; Al Qabany and Soga 2013; Martinez et al. 2013; Montoya et al. 2013). During this injection procedure, bacterial suspension was initially injected into a soil matrix and subsequently left to 'settle' for several hours to enable bacteria to attach to the inner surface of the porous medium before the injection of the cementation solution. Normally, the injection of cementation solution was conducted in stages with an injection interval of 3-24 hours between two subsequent injections. The glass slide experiment cannot simulate the flow of bacterial suspension and cementation solution through a porous soil matrix, which may affect the distribution of bacterial aggregates and individual bacterial cells, and which in turn may affect the properties of MICP-treated soils. In addition, in the glass slide experiment, bacterial suspension

and cementation solution can only be mixed once, whereas in real MICP applications the injection of cementation solution is normally repeated multiple times to increase the amount of $CaCO_3$ formed (van Paassen et al. 2010; Al Qabany et al. 2012). Therefore, after performing the glass slide experiments, microfluidic chip experiments were conducted to further explore the MICP process under conditions that more closely mimic MICP conditions that are present in real soils.

The schematic of the setup for the microfluidic chip experiments and the two-dimensional design of the microfluidic chip are shown in Figure 3. The microfluidic chip was designed to create a two-dimensional model of the porous structure of a soil matrix based on a cross-sectional image of a solidified and sectioned three-dimensional Ottawa 30-50 sandy soil specimen and was fabricated using standard photolithography techniques. A cover slip made of polydimethylsiloxane (PDMS) which contained a matrix of irregularly-shaped pillars was bonded to a piece of glass slide by plasma treatment to create porous channels with pores to enable flow between the pillars (Figure 3a). Most of the distances between two adjacent pillars were shorter than 50 microns, roughly equivalent to the depth of the porous medium inside the microfluidic chip. Based on a two-dimensional design of the microfluidic chip, the calculated porosity of the porous medium inside the microfluidic chip was approximately 0.40 (Figure 3b). The microfluidic chip also contained an inlet and an outlet to inject and let out the solution, respectively. Upstream flow distribution channels and downstream flow distribution channels were used to homogeneously distribute the flow in and out of the porous medium (Figure 3b). A more detailed description of the design and fabrication process of the PDMS cover slip is given in Wang et al. (2018). The experiments were conducted using both the microfluidic chip and a liquid injection system, which comprised a syringe, a syringe pump and tubing. The injection system was used to inject the bacterial

suspension and cementation solution into the microfluidic chip. The microfluidic chip is optically transparent, and the bacterial cells and the calcium carbonate inside the microfluidic chip can be observed under a high resolution optical microscope.

Staged injection MICP procedures were applied in three microfluidic chip experiments. The parameters of bacterial suspension and bacterial injection were the same in these three experiments. The OD_{600} of the bacterial suspension measured prior to the bacterial injection was 1.0. The injection flow rate of bacterial suspension was 0.5 ml/h and the calculated Darcy velocity is 4.6×10^{-4} m/s at this injection flow rate. The volume of the bacterial suspension injected (11.25 μl) was 1.25 times higher than the pore volume of the microfluidic chip (9 μl). After the injection of bacterial suspension, the bacteria were given 24 hours to attach to the inner surface of the porous medium prior to the injection of cementation solution. The cementation solution used in all of the three microfluidic chip experiments was constant and contained 0.25 M $CaCl_2$, 0.375 M urea, and 3 g/L nutrient broth. In addition, the volume of the cementation solution injected during each injection was also constant, which was 1.25 times higher than the pore volume of the microfluidic chip. However, the other parameters associated with the cementation solution injection were varied in the three experiments and are summarized in Table 2. In the first experiment, two injection flow rates of cementation solution were applied, which were 0.05 ml/h and 0.5 ml/h, corresponding to Darcy velocities of 4.6×10^{-5} m/s and 4.6×10^{-4} m/s, respectively. This experiment was conducted to explore the behavior of bacteria after injecting cementation solution at different flow rates. In the second experiment, two injections of cementation solution were applied to explore whether the $CaCO_3$ precipitation occurs after the first and the second injections of the cementation solution in the same way as observed in the glass slide experiment. The third experiment was conducted to

explore whether different MICP treatment procedures produce $CaCO_3$ crystals with different sizes when the injection interval between two successive injections of cementation solution is varied. In this experiment, 12 injections of cementation solution were applied, with intervals of either (i) 3-5 hours or (ii) 23-25 hours between successive injections. For each protocol, a newly fabricated microfluidic chip was used.

Micro-scale visualization and image quantification

Images of samples were taken using an optical microscope (Zeiss Axio Observer.Z1) to visualize the bacterial cells and $CaCO_3$ precipitates. The microscope was equipped with a black and white camera (Hamamatsu C11440-22CU) connected to a computer. Images were taken using phase field illumination and 10× inverted objective with an image resolution of 0.65 μm/pixel. The image of $CaCO_3$ precipitates is brighter than both bacterial cells and the solution under the optical microscope in phase field. To quantify the size of individual crystals, the diameters or lengths of the crystals in the 2-D images were measured using ZEN software (Zeiss). The number of crystals present in selected areas of the images were also counted to quantify the number of crystals formed in a unit area.

RESULTS OF MICROSCOPE SLIDE EXPERIMENTS AND DISCUSSION

Bacterial aggregation

In the first glass slide experiment, microscope images of several samples containing bacterial suspension or mixtures of bacterial suspension with each of the main components of cementation solution were captured and compared with images taken after mixing bacterial suspension with cementation solution (shown in Figure 4). Figure 4a shows the image of a sample containing *S.*

pasteurii suspension. The *S. pasteurii* cells were about 3 μm in length and were rod-shaped, which is consistent with the size and shape of *S. pasteurii* cells observed by scanning electron microscopy (Bang et al. 2001; Keykha et al. 2013). The *S. pasteurii* cells did not aggregate in the bacterial suspension (Figure 4a). This might be due to the repulsive forces between bacterial cells. In the presence of cementation solution, the bacteria aggregated (Figure 4a compared with 4b), which is consistent with the images shown by van Paassen (2009). In addition, *S. pasteurii* cells aggregated in the presence of $CaCl_2$ (Figure 4c), but not in the presence of urea or nutrient broth (Figure 4d and e). This suggests that the $CaCl_2$ contained in the cementation solution is the component that induced bacterial aggregation, which is consistent with previous findings reported in the literature (El Mountassir et al. 2014).

The evolution of $CaCO_3$ precipitate size and shape during MICP

Time series images of the mixture of bacterial suspension and cementation solution which were taken over twelve hours are shown in Figure 5. Bacterial aggregation and $CaCO_3$ precipitation started immediately after the mixing (Figure 5a), which is consistent with the observation made by van Paassen (2009). The shapes of both bacterial aggregates and $CaCO_3$ precipitates at the initial stage were irregular (Figure 5a). By 30 minutes after mixing, more irregularly-shaped $CaCO_3$ precipitates formed (Figure 5b), shown by more areas in the image becoming brighter at 30 min compared with 0 min. The irregularly-shaped $CaCO_3$ precipitates continued growing until 50 minutes when one spherical $CaCO_3$ crystal (crystal A) appeared (circular in the 2-D image, Figure 5c). After that, the irregularly-shaped $CaCO_3$ precipitates surrounding crystal A started dissolving. The area containing dissolving irregularly-shaped $CaCO_3$ became larger with the growth of crystal A (Figure 5e compared with Figure 5d). In the meantime, several new crystals formed (Figure 5e

compared with Figure 5d). It is worth noting that the zones where the irregularly-shaped $CaCO_3$ precipitates dissolved were not only increasing in size with the growth of the crystals, but also had a circular shape (Figure 5f-h). By 1 h and 45 minutes, some undissolved irregularly-shaped $CaCO_3$ precipitates (Figure 5i) remained, but by 2 hours all dissolved (Figure 5j). Between 2 - 12 hours, all of the existing $CaCO_3$ precipitates were regularly-shaped crystals (Figure 5j-l). Therefore, in general, the overall MICP process between 0-12 hours after the mixing of bacterial suspension and cementation solution can be divided into the following three main stages: (1) bacterial aggregation which occurs immediately after the mixing of bacterial suspension with cementation solution; (2) growth of irregularly-shaped $CaCO_3$ precipitates (0-1 hr); and (3) dissolution of irregularly-shaped $CaCO_3$ precipitates (1-2 hr) at the expense of the growth and formation of regularly-shaped $CaCO_3$ crystals (1-12 hr).

The irregularly-shaped $CaCO_3$ precipitates formed during the initial stage of $CaCO_3$ precipitation were not stable and dissolved easily with the precipitation of the regularly-shaped $CaCO_3$ crystals, which is consistent with the observations made by Kawano et al. (2002). According to Ostwald's step rule, amorphous $CaCO_3$ (ACC), which is the most unstable form of $CaCO_3$, is the first to precipitate during $CaCl_2$- and Na_2CO_3 - induced chemical precipitation of $CaCO_3$. This is because ACC has the highest solubility among all the $CaCO_3$ precipitates, and because the concentrations of Ca^{2+} and CO_3^{2-} in the mixed solution drop to the solubility for ACC during its precipitation, whilst still being high enough for more stable $CaCO_3$ crystals such as vaterite and calcite to nucleate and grow (Kawano et al. 2002). In our study, the $CaCO_3$ precipitates which formed first were irregularly-shaped and had higher solubility compared with the crystal form of $CaCO_3$ precipitates, which is consistent with the parameters of amorphous phase $CaCO_3$ (Kawano et al.

2002; Bots et al. 2012; Dhami et al. 2013; Rodriguez-Blanco et al. 2011). In addition, the irregularly-shaped $CaCO_3$ precipitates dissolved around the crystals that formed, the shapes of the zones where the irregularly-shaped $CaCO_3$ precipitates dissolved were circular, and these areas increased with the growth of the $CaCO_3$ crystals. These observations also suggest that the crystals grew at the expense of the dissolution of the irregularly-shaped $CaCO_3$ precipitates (Kawano et al. 2002). The $CaCO_3$ precipitation process observed in this study is consistent with the process observed by Kawano et al. (2002), in which unstable $CaCO_3$ precipitated first and then dissolved when more stable crystals precipitated. However, the precipitation of $CaCO_3$ in the study by Kawano et al. (2002) was caused by the chemical reaction between $CaCl_2$ and Na_2CO_3, rather than by biochemical reactions due to bacterial activity.

As the magnification level in the images shown in Figure 5 is not high enough to observe the details of bacterial cells and $CaCO_3$ crystals, images taken at higher magnification levels (squares I and II in Figure 5) are shown in the next two subsections to observe more details regarding the precipitation and dissolution of irregularly-shaped $CaCO_3$ precipitates and the evolution of $CaCO_3$ crystals.

i. Precipitation and dissolution of irregularly-shaped $CaCO_3$ crystals

Magnified images of square I shown in Figure 5a at selected time points (0 min, 20 min and 50 min) are shown in Figure 6a-c to observe whether individual bacterial cells or bacterial aggregates have an effect on the nucleation and growth of $CaCO_3$ precipitates. To observe the images in more detail, magnified images of the square in Figure 6a-c are shown in Figure 6d-f.

A large amount of the bacterial cells aggregated and irregularly-shaped $CaCO_3$ precipitates started forming immediately after the start of the imaging process (Figure 6a). The irregularly-shaped $CaCO_3$ precipitates formed mostly on bacterial aggregates (Figure 6b, indicated by the arrows) and occasionally also formed on individual bacterial cells (Figure 6f, indicated by the arrows). The $CaCO_3$ precipitates continued to grow from 0 to 50 min, as shown by the image pixels becoming brighter (Figure 6b compared with Figure 6a, or Figure 6c compared with Figure 6b). The time at which the precipitates started forming varied, with some of these forming at 0 minutes, whereas others formed after 20 minutes.

The images in Figure 6 suggest that bacterial aggregation affects the formation of irregularly-shaped $CaCO_3$ precipitates. Based on equations 1 and 2, bacteria hydrolyze urea and produce CO_3^{2-} ions which react with Ca^{2+} to form $CaCO_3$. Assuming that the ureolysis capacity of each bacterial cell is the same, bacterial aggregates containing a large number of bacteria are more effective at hydrolyzing urea compared to individual bacterial cells. Therefore, the concentration of CO_3^{2-} surrounding the bacterial aggregates increases more quickly. In addition, the bacterial aggregates contained a large amount of Ca^{2+} surrounding the bacterial cells, thus causing $CaCO_3$ to precipitate on bacterial aggregates more quickly. As the local concentration of urea surrounding the bacterial aggregates decreases, more urea diffuses to them, thus resulting in the continued precipitation of $CaCO_3$ on the bacterial aggregates.

This observation suggests that bacterial aggregates formed during the initial stage of $CaCO_3$ precipitation and that they had an effect on $CaCO_3$ precipitation where the precipitates grew on top of bacterial aggregates. In addition, individual bacterial cells affected the precipitation of

irregularly-shaped $CaCO_3$ precipitates, but the effect of individual bacterial cells is less compared with the effect of bacterial aggregates.

To observe the dissolution of irregularly-shaped $CaCO_3$ precipitates in more detail, magnified images of square II (shown in Figure 5a) at selected time points (between 30 min and 2 hrs) are shown in Figure 7. With the dissolution of the $CaCO_3$ precipitate, the bacterial cells become free to move. *S. pasteurii* belongs to the genus Bacillus and the mobility of *S. pasteurii* is consistent with that of Bacillus bacteria (Yoon et al. 2001). These observations suggest that bacterial aggregation and the formation of irregularly-shaped $CaCO_3$ precipitates encapsulate bacterial cells. By contrast, because the irregularly-shaped $CaCO_3$ precipitates were not stable, the dissolution of the irregularly-shaped $CaCO_3$ resulted in the bacterial cells becoming free to move again.

ii. Dissolution of irregularly-shaped $CaCO_3$ and re-precipitation of $CaCO_3$ crystals

To observe the precipitation process and stabilities of $CaCO_3$ crystals in more detail, including the evolution of their shape and size, magnified images of square I in Figure 5a at selected time points are shown in Figure 8. As can be seen from this figure, $CaCO_3$ crystals grew with the dissolution of the irregularly-shaped $CaCO_3$ precipitates. Most crystals were spherical, such as crystals A-F, or rhombohedral, such as crystals G-Q. The spherical and rhombohedral shapes of $CaCO_3$ crystals are consistent with the shapes of vaterite and calcite, respectively (Kawano et al. 2002; Chu et al. 2013). Spherical crystals were not stable and dissolved later on. For example, crystal B dissolved by 12 hours and crystals C - F dissolved by 7 hours. Rhombohedral crystals such as crystals G-Q were stable and did not dissolve after being formed.

To observe the formation of spherical and rhombohedral $CaCO_3$ crystals in more detail, such as changes in their shape and size with time, magnified images of crystals C and I, which are shown in Figure 8, were selected to be representative and their shapes at selected time points are shown in Figures 9 and 10, respectively.

The spherical crystal C started to form by 1 hr 25 min (Figure 9d), and then grew until 2 hrs (Figure 9f), after which it started to dissolve and became fully dissolved by 7 hrs (Figure 9o). Therefore, spherical crystal C is relatively unstable. This dissolution of spherical crystals is consistent with the dissolution of vaterite according to Ostwald's step rule, as well as with the SEM images showing the dissolved vaterite (van Paassen 2009) taken 1 week after MICP treatment. In contrast, the rhombohedral crystal (crystal I) was stable once it was formed (Figure 10d-l).

These results are consistent with several studies where the percentage of rhombohedral $CaCO_3$ crystals relative to all crystals increased at later stages during the precipitation process (Wei et al. 2003; Rodriguez-Blanco et al. 2011). However, the results presented in this study are the first direct observation of the process of dissolution of spherical $CaCO_3$ crystals at an expense of further growth of rhombohedral crystals.

RESULTS OF MICROFLUIDIC CHIP EXPERIMENTS AND DISCUSSION

The $CaCO_3$ precipitation process shown in the glass slide experiment represents the process occurring after the bacterial suspension was mixed with the cementation solution. However, this does not fully represent the actual MICP process in which the bacterial suspension and cementation

solution are successively injected into a soil matrix (DeJong et al. 2006; Al Qabany and Soga 2013; Martinez et al. 2013; Montoya et al. 2013). The objectives of the microfluidic experiments were: (1) to observe bacterial aggregation during sequential injections of bacterial suspension and cementation solution; (2) to observe $CaCO_3$ crystal formation after each of the cementation solution injections; (3) to examine the movement of $CaCO_3$ precipitates with the flow; and (4) to investigate various MICP treatment procedures during which the time interval between successive injections of cementation solution was varied, to establish a correlation between the $CaCO_3$ precipitation processes and the final size of $CaCO_3$ crystals.

Bacterial behavior after staged injections of bacteria and cementation solution

The first microfluidic experiment was conducted to observe bacterial aggregation during a staged-injection MICP process. Two protocols (protocols 1_1 and 1_2) were applied and the experimental parameters are summarized in Table 2. The difference between these two protocols is the injection flow rate of cementation solution, which were 0.05 ml/h and 0.5 ml/h, corresponding to Darcy velocities of 4.6×10^{-5} m/s and 4.6×10^{-4} m/s, respectively. These values are within the range of values reported in the literature (Al Qabany and Soga 2013; Martinez et al. 2013; Montoya et al. 2013).

Bacterial cells continued to grow even after being injected as shown by the difference in the number of bacteria present between Figure 11a_1 and Figure 11a_2. A large proportion of bacterial cells were flushed out after the injection of cementation solution (Figure 11b_1 or b_2 compared with 11a_2). In an open pore, fewer bacterial cells remained after the injection of cementation solution when the injection flow rate of cementation solution was ten times higher (Figure 11b_1

compared with b_2). On the other hand, bacterial aggregation and precipitation of irregularly-shaped $CaCO_3$ occurred after the injection of cementation solution either in narrow pore throats or on vertical surfaces within the microfluidic chips at both flow rates (Figure 11b_3 and b_4). The bacteria fixed by the irregularly-shaped $CaCO_3$ crystals were no longer aggregated by 24 hours (Figure 11c_1 and c_2).

The results of this experiment suggest that the bacterial cells did not aggregate after injection or after settling, but that some of them aggregated after the injection of cementation solution, even though this aggregation was less extensive compared with the bacterial cells which aggregated in the mixture of bacterial suspension and cementation solution in the glass slide samples. This is because bacterial cells were relatively well mixed with the Ca^{2+} ions of the cementation solution in a glass slide sample, which resulted in relatively large quantities of bacterial aggregates. However, in the staged-injection microfluidic chip experiment, the bacterial cells were only aggregated by Ca^{2+} at the interface between the bacterial suspension and cementation solution, where bacterial cells dispersed into the cementation solution and Ca^{2+} diffused into the bacterial suspension. The injection of cementation solution pushed the interface between these two liquids forward towards the outlet of the microfluidic chip, with bacterial aggregates becoming filtered or adsorbed by the porous medium during the injection of cementation solution. Flow rate affects bacterial detachment at open pores, where fewer bacteria remained after the injection of cementation solution when the flow rate was higher (0.5 ml/h, calculated Darcy velocity is 4.6×10^{-4} m/s) compared with a flow rate of 0.05 ml/h. However, because bacterial aggregates became trapped within the narrow pores after the injection of cementation solution at both flow rates (0.5

ml/h and 0.05 ml/h), the number of bacteria remaining in the porous medium after the injection of cementation solution was similar at both flow rates.

Crystal formation after injection of cementation solution

The second microfluidic chip experiment was conducted to examine the $CaCO_3$ precipitation process during an MICP procedure involving a single injection of bacterial suspension followed by two subsequent injections of cementation solution. Figure 12 shows the time series images of five pores in the microfluidic chip taken directly after the first injection of cementation solution, and at 1 hour, 3 hours, and 24 hours after the injection. Consistent with the results obtained from the glass slide experiment, bacterial cells aggregated, although to a smaller extent compared to that in the glass slide experiment (see Figure 12, pore I, II, III and V, 0 hr photos). Furthermore, irregularly-shaped $CaCO_3$ precipitates were formed (see Figure 12, pore I, II, III and V, 0 hr photos). The irregularly-shaped $CaCO_3$ precipitates continued to grow from 0 to 1 hour (see Figure 12, pore I, II, III and V, 1 hr photos compared with 0 hr photos) and then dissolved (see Figure 12, pore I, II 3 hr photos; pores III, V, 24 hr photos compared with 0 hr photos). With the dissolution of the irregularly-shaped $CaCO_3$ precipitates, the bacterial cells that were enclosed became dispersed (see Figure 12, pore I, II, 3 hr photos). $CaCO_3$ crystals appeared with the dissolution of the irregularly-shaped $CaCO_3$ precipitates (such as pore V, 3 hr photo compared with 1 hr photo). Finally, the spherical crystals dissolved but the other crystals remained (such as pore IV, 24 hrs photo).

In Figure 13, images of Pore V at 0, 1, 3 and 24 hours after the completion of the second injection of cementation solution are presented. The two crystals formed after the first injection of

cementation solution were still at the same place inside the pore after the second injection of cementation solution. This suggests that the crystals were stable inside the porous medium and could not be flushed out at a flow rate of 0.05 ml/h. At 3 hours, small crystals formed (bright dots in Figure 13). However, by 24 hours, the small crystals dissolved. The big crystals in these two pores continued to grow during the first 24 hours, after which only the big crystals and several newly formed crystals remained.

Effect of injection interval on the size of $CaCO_3$ crystals

The results from the second microfluidic chip experiment suggest that the unstable $CaCO_3$ crystals dissolved at the expense of the growth of more stable crystals after the first and second injection of cementation solution. The dissolution of the unstable crystals occurred between 3 and 24 hours after each of the injections, suggesting that the final crystal size would be different if the injection interval was to be shorter than 24 hours. The third microfluidic chip experiment was conducted by varying the time interval between subsequent injections of cementation solution. The experimental parameters are shown in Table 2. The first protocol (protocol 3_1) had a short injection interval (3-5 hour interval and injected 2-4 times per day), whereas the second protocol (protocol 3_2) had a longer interval of 23-25 hours (injected once per day). The images which were taken at the middle of the two microfluidic chips one day after the final (the 12^{th}) injection of cementation solution are shown in Figure 14a. Magnified images of the two squares in these two images depicted in Figure 14a are shown in Figure 14b to show the crystals in more detail.

The left images in Figure 14a and b show the crystals formed during the short injection interval protocol (protocol 3_1). The sizes of spherical crystals were small (5 - 10 μm) but the number of

crystals was high (200 - 1000 per 10^6 μm^3) (Figure 14a and b, left images). The crystals coated the inner surface of the microfluidic chip. Small crystals remained inside the pores because a 3-5 hour retention time was not long enough for every small crystal to dissolve.

The right images in Figure 14a and b show the crystals formed during the long injection interval protocol (protocol 3_2). The sizes of $CaCO_3$ crystals are larger (10 - 80 μm) than those in protocol 3_1. The number of crystals inside the pores is small (5 - 20 per 10^6 μm^3), which is about 40 times smaller than the number of crystals observed in protocol 3_1. A 23-25-hour retention time resulted in smaller spherical crystals being dissolved, and the calcium cations which were produced by this dissolution process formed larger crystals.

Al Qabany et al. (2012) concluded that the size of $CaCO_3$ crystals formed was smaller when soil samples were treated more frequently with a lower concentration of cementation solution compared with soil samples that were treated less frequently with a higher concentration of cementation solution. In light of this finding, our results suggest that when the concentration of cementation solution is constant, the treatment frequency and interval between injections also affect the final size of the crystals. That is, a longer injection interval produces larger crystals. Because crystal size may affect engineering properties such as strength and permeability, this might be a reason why the engineering properties of the MICP-treated samples varied when the properties of soil treated and the $CaCO_3$ content produced are the same. It was suggested that large crystals which precipitated at grain contacts that can bond soil particles helps to increase the strength of MICP treated-soils (DeJong et al. 2010). In addition, research has recommended that the formation of stable $CaCO_3$ is important for improving the stability of MICP-treated soils (van

Paassen 2009). Therefore, based on these results, a long injection interval (23 - 25 hours) might be better compared with a shorter injection interval (3 - 5 hours). This is because when the injection interval is shorter (3 - 5 hours), the crystals are small and coated the surface of the soil particles, whereas when the injection interval is longer (23 - 25 hours), the crystals are larger in size and are more likely to effectively bond the soil particles. Further work is needed to establish a relationship between crystal size and injection intervals based on the findings made in this study, as well as to determine the effect of injection intervals on the engineering properties of MICP-treated samples.

CONCLUSIONS

In this study, the MICP process was visualized at the micro-scale in order to understand the effects of bacterial cells on $CaCO_3$ precipitation, the evolution of the shape and size of the $CaCO_3$ precipitates during the MICP process, and the effect of treatment procedure on the final size of $CaCO_3$ crystals. The main findings of this study are summarized as follows.

Bacterial aggregation was first observed in the glass-slide experiments in the mixture of bacterial suspension and cementation solution. Such aggregation was also observed in the staged-injection microfluidic chip experiments after injection of the cementation solution, even though less aggregation was observed than in the glass slide experiment. Bacterial aggregation is an important factor promoting the fixing of bacterial cells in the chip and $CaCO_3$ precipitation where the precipitates grew on top of bacterial aggregates.

Both glass-slide experiments and microfluidic experiments show that the shape and size of the $CaCO_3$ precipitates change during the MICP process. At first, irregularly-shaped $CaCO_3$

precipitates form during the initial stage of the precipitation process. These precipitates then dissolve as $CaCO_3$ crystals (spherical or rhombohedral) form. At longer time-scales, spherical $CaCO_3$ crystals dissolve at the expense of the growth of rhombohedral $CaCO_3$ crystals. Likewise, small crystals tend to dissolve at the expense of the growth of larger $CaCO_3$ crystals of the same type.

The rhombohedral crystals appear to be more stable than the spherical crystals, which in turn are more stable than the irregularly-shaped precipitates. This is reminiscent of the transformation of irregularly-shaped amorphous $CaCO_3$ precipitates to spherical vaterite and then to rhombohedral calcite (Rodriguez-Blanco et al. 2011). Together with the morphological aspects of these structures, we can assume that rhombohedral crystals are calcite, spherical crystals are vaterite, and irregularly-shaped precipitates are amorphous $CaCO_3$ precipitates, as suggested by Rodriguez-Blanco et al. (2011) and Chu et al. (2013). Such transformations are common aspects of $CaCO_3$ physical chemistry and must therefore be robust features of MICP in the microfluidic device and in larger-scale applications.

The time-dependent phase transformation of $CaCO_3$ precipitates makes the produced MICP crystal size highly dependent on the time interval between cementation solution injections during a staged injection procedure. The average size of $CaCO_3$ crystals was considerably higher when the injection interval was 23 - 25 hours instead of 3 - 5 hours.

This work demonstrates that, even though the total amount of $CaCO_3$ might be the same, the size of $CaCO_3$ crystals may be different when different injection intervals are used. This difference

would in turn affect the engineering properties of MICP-treated samples such as permeability, stiffness, and strength. All of the cementation inside soils decreases permeability, and large crystals at the open pore throat might correspond to the effective $CaCO_3$ required to reduce soil permeability (Al Qabany and Soga 2013). The production of larger crystals at narrow pore throats that are able to bond soil particles might be more efficient in increasing the stiffness and strength of MICP-treated soils (DeJong et al. 2010). Further work involving translation of these findings to real soil applications will be useful for determining a relationship between the treatment process and the engineering properties of MICP-treated soils.

The general approach presented here also opens the door to a systematic and quantitative study of other factors likely to affect bacterial aggregation and $CaCO_3$ precipitation process. The size and shape of the pores, as well as the surface properties of the porous medium can be experimentally controlled to study how soil-specific attributes may influence MICP. Environmental parameters such as temperature would also influence the resulting precipitation dynamics. We anticipate that *in vitro* studies of $CaCO_3$ combining microfluidics and imaging will play an important role in optimizing MICP for a broad range of soils and climates.

ACKNOWLEDGMENTS

The first author would like to acknowledge Cambridge Commonwealth, European and International Trust, and China Scholarship Council for financially supporting this research project.

ABBREVIATIONS

MICP, Microbial-Induced Calcium Carbonate Precipitation; BS, bacterial suspension; CS, cementation solution; BA, bacterial aggregate; ISP, irregularly-shaped precipitate; OD_{600}, optical density measured at a wave length of 600 nm; PDMS, polydimethylsiloxane; *S. pasteurii, Sporosarcina pasteurii*

REFERENCES

Al Qabany, A., Soga, K., and Santamarina, C. (2012). "Factors affecting efficiency of microbially induced calcite precipitation." *J. Geotech. Geoenviron. Eng.,* 138(8): 992-1001.

Al Qabany, A., and Soga, K. (2013). "Effect of chemical treatment used in MICP on engineering properties of cemented soils." *Géotechnique*, 63(4), 331–339.

Bots, P., Benning, L. G., Rodriguez-Blanco, J.-D., Roncal-Herrero, T., and Shaw, S. (2012). "Mechanistic insights into the crystallization of amorphous calcium carbonate (ACC)." *Crystal Growth and Design*, 12(7), 3806–3814.

Bang, S. S., Galinat, J. K., and Ramakrishnan, V. (2001). "Calcite precipitation induced by polyurethane-immobilized Bacillus pasteurii." *Enzyme Microb. Technol.*, 28, 404–409.

Carteret, C., Dandeu, A., Moussaoui, S., Muhr, H., Humbert, B., and Plasari, E. (2009). "Polymorphism Studied by Lattice Phonon Raman Spectroscopy and Statistical Mixture Analysis Method. Application to Calcium Carbonate Polymorphs during Batch Crystallization." *Crystal Growth and Design*, 9(2), 807–812.

Cheng, L., Shahin, M. A., and Mujah, D. (2017). "Influence of Key Environmental Conditions on Microbially Induced Cementation for Soil Stabilization." *J. Geotech. Geoenviron. Eng.*, 143(1), 04016083.

Chu, D. H., Vinoba, M., Bhagiyalakshmi, M., Hyun Baek, I., Nam, S. C., Yoon, Y., and Jeong, S. K. (2013). "CO_2 mineralization into different polymorphs of $CaCO_3$ using an aqueous-CO_2 system." *RSC Advances*, 3(44), 21722.

Cöelfen, H., and Antonietti, M. (2008). "Mesocrystals and nonclassical crystallization." John Widley & Sons, Ltd.

DeJong, J. T., Fritzges, M. B., and Nüsslein, K. (2006). "Microbially Induced Cementation to Control Sand Response to Undrained Shear." *J. Geotech. Geoenviron. Eng.,* 132(11), 1381–1392.

DeJong, J. T., Mortensen, B. M., Martinez, B. C., and Nelson, D. C. (2010). "Bio-mediated soil improvement." *Ecol. Eng.,* 36(2), 197–210.

Dhami, N. K., Reddy, M. S., and Mukherjee, A. (2013). "Biomineralization of calcium carbonates and their engineered applications: a review." *Frontiers in Microbiology, 4(October), 314.*

El Mountassir, G., Lunn, R. J.; Moir, H., and MacLachlan, E. (2014). "Hydrodynamic coupling in microbially mediated fracture mineralization: Formation of self-organized groundwater flow channels." *Water Resour. Res.* 50 (1), 1–16.

Ganendra, G., De Muynck, W., Ho, A., Arvaniti, E. C., Hosseinkhani, B., Ramos, J. A., and Boon, N. (2014). "Formate oxidation-driven calcium carbonate precipitation by Methylocystis parvus OBBP." *Appl. Environ. Microbiol.*, *80*(15), 4659–67.

Hammes, F., and Verstraete, W. (2002). "Key roles of pH and calcium metabolism in microbial carbonate precipitation." *Re/Views in Environmental Science and Bio/Technology* 1(1), 3–7.

Jiang, N.-J., Soga, K., and Kuo, M. (2017). "Microbially Induced Carbonate Precipitation for Seepage-Induced Internal Erosion Control in Sand–Clay Mixtures." *J. Geotech. Geoenviron. Eng.,* 10.1061/(ASCE)GT.1943-5606.0001559, 04016100.

Kawano, J., Shimobayashi, N., Kitamura, M., Shinoda, K., and Aikawa, N. (2002). "Formation process of calcium carbonate from highly supersaturated solution." *Journal of Crystal Growth*, *237–239*(1–4 I), 419–423.

Keykha, H. A., Zareian, M., Huat, B. B. K., Asadi, A., and Kawasaki, S. (2015). Electrokinetic properties of pasteurii and aquimarina bacteria. *Environmental Geotechnics*, 2 (3), 181-188

Lin, H., Suleiman, M. T., Brown, D. G., and Kavazanjian, E. (2016). Mechanical Behavior of Sands Treated by Microbially Induced Carbonate Precipitation. *J. Geotech. Geoenviron. Eng.,* 142(2): 04015066

Lian, B., Hu, Q., Chen, J., Ji, J., and Teng, H. H. (2006). Carbonate biomineralization induced by soil bacterium Bacillus megaterium. *Geochim. Cosmochim. Acta*, *70*(22), 5522–5535.

Martinez, B. C., DeJong, J. T., Ginn, T. R., Montoya, B. M., Barkouki, T. H.; Hunt, C., Tanyu, B., and Major, D. (2013). "Experimental Optimization of Microbial-Induced Carbonate Precipitation for Soil Improvement." *J. Geotech. Geoenviron. Eng.,* 139 (4), 587–598.

Mitchell, A. C., and Ferris, F. G. (2006). "The Influence of Bacillus pasteurii on the Nucleation and Growth of Calcium Carbonate." *Geomicrobiol. J.*, *23*(November), 213–226.

Morse, J. W., Arvidson, R. S., and Lüttge, A. (2007). "Calcium carbonate formation and dissolution." *Chemical Reviews*, *107*(979), 342–381.

Montoya, B. M., DeJong, J. T., and Boulanger, R. W. (2013). "Dynamic response of liquefiable sand improved by microbial-induced calcite precipitation." *Géotechnique*, 63 (4), 302–312.

Ogino, T., Suzuki, T., and Sawada, K. (1987). "The formation and transformation mechanism of calcium carbonate in water." *Geochim. Cosmochim. Acta*, *51*(10), 2757–2767.

Phillips, A. J., Lauchnor, E., Eldring, J., Esposito, R., Mitchell, A. C., Gerlach, R., and Spangler, L. H. (2013). "Potential CO_2 leakage reduction through biofilm-induced calcium carbonate precipitation." *Environ. Sci. Technol.*, 47(1), 142–149.

Rodriguez-Blanco, J. D., Shaw, S., and Benning, L. G. (2011). "The kinetics and mechanisms of amorphous calcium carbonate (ACC) crystallization to calcite, via vaterite." *Nanoscale*, 3(1), 265–271.

Stocks-Fischer, S., Galinat, J. K., and Bang, S. S. (1999). "Microbiological precipitation of $CaCO_3$." *Soil Biol. Biochem.*, 31(11), 1563–1571.

van Paassen, L. (2009*)*. "Biogrout: Ground Improvement by Microbially Induced Carbonate Precipitation." PhD Thesis. Delft University of Technology, Delft, the Netherlands.

van Paassen, L. A., Ghose, R., van der Linden, T. J. M., van der Star, W. R. L., and van Loosdrecht, M. C. M. (2010). "Quantifying Biomediated Ground Improvement by Ureolysis: Large-Scale Biogrout Experiment." *J. Geotech. Geoenviron. Eng.,* 136(12), 1721–1728.

Whiffin, V. S., van Paassen, L. A., and Harkes, M. P. (2007). "Microbial Carbonate Precipitation as a Soil Improvement Technique." *Geomicrobiol. J.*, *24*(5), 417–423.

Wang, Y., Soga, K., and Jiang N.-J. (2017). "Microbial induced carbonate precipitation (MICP): the case for microscale perspective." In *Proceedings of the 19th International Conference on Soil Mechanics and Geotechnical Engineering*, 1099-1102, Seoul, Korea.

Wang, Y., Soga, K., DeJong, J. T., and Kabla, A. J. (2018). "A microfluidic chip and its use in characterizing the particle-scale behavior of Microbial-Induced Carbonate Precipitation (MICP)." *Géotechnique,* https://doi.org/10.1680/jgeot.18.p.031.

Wei, H., Shen, Q., Zhao, Y., Wang, D. J., and Xu, D. F. (2003). "Influence of polyvinylpyrrolidone on the precipitation of calcium carbonate and on the transformation of vaterite to calcite." *Journal of Crystal Growth*, 250(3–4), 516–524.

Yoon, J. H., Lee, K. C., Weiss, N., Kho, Y. H., Kang, K. H., and Park, Y. H. (2001). "Sporosarcina aquimarina sp. nov., a bacterium isolated from seawater in Korea, and transfer of Bacillus globisporus (Larkin and Stokes 1967), Bacillus psychrophilus (Nakamura 1984) and Bacillus pasteurii (Chester 1898) to the genus Sporosarcina as Sporosa." *International Journal of Systematic and Evolutionary Microbiology*, 51(3), 1079–1086.

Zhou, G. T., Yu, J. C., Wang, X. C., and Zhang, L. Z. (2004). "Sonochemical synthesis of aragonite-type calcium carbonate with different morphologies." *New J. Chem.* 28(8), 1027–1031.

Table 1. Parameters of glass slide experiments

Experiment No.	Sample No.	Content 1	Content 2
1	a	BS (OD_{600} = 1)	-
	b	BS (OD_{600} = 1)	CS (1 M)
	c	BS (OD_{600} = 1)	1 M $CaCl_2$
	d	BS (OD_{600} = 1)	1.5 M urea
	e	BS (OD_{600} = 1)	3 g/L nutrient broth
2	-	BS (OD_{600} = 2.5)	CS (1 M)

Note: BS- bacterial suspension; CS- cementation solution; CS (1 M) contains 1 M $CaCl_2$, 1.5 M urea, and 3 g/L nutrient broth

Table 2. Parameters of cementation solution injection in the microfluidic chip experiments

Experiment No.	1		2	3	
Protocol No.	1_1	1_2	2	3_1	3_1
Flow rate (ml/hour)	0.05	0.5	0.05	0.05	0.05
Injection number	1	1	2	12	12
Injection frequency per day	-	-	once	2-4 times	once
Injection intervals (hour)	-	-	24	3-5	23-25
Total treatment duration (day)	-	-	2	4	12

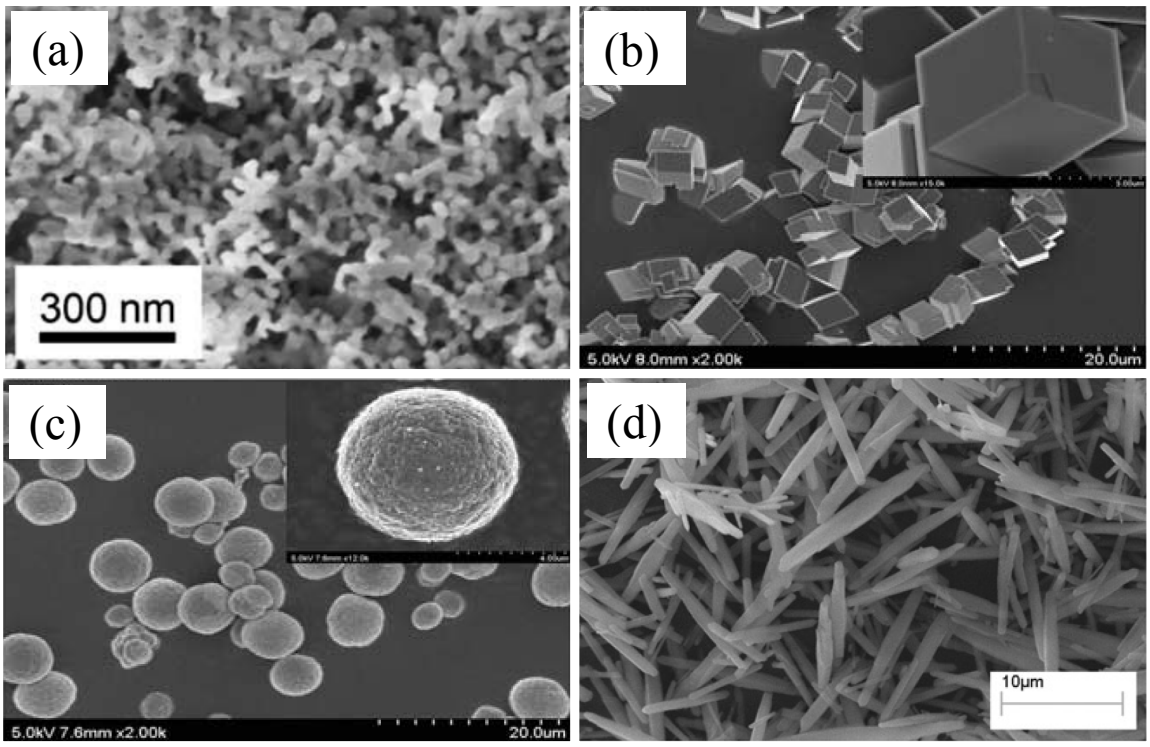

Fig. 1. Polymorphs of $CaCO_3$. (a) amorphous calcium carbonate (ACC) (Rodriguez-Blanco et al. 2011); (b) calcite (Chu et al. 2013); (c) vaterite (Chu et al. 2013); (d) aragonite (Zhou et al. 2004)

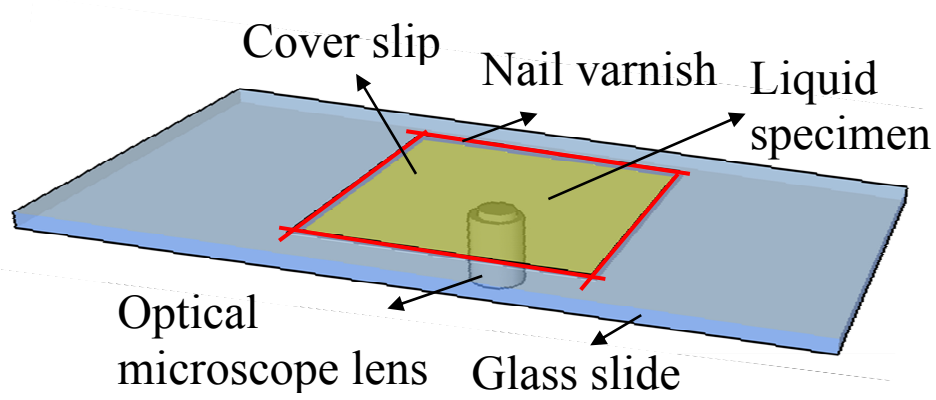

Fig. 2. Schematic of setup for glass slide experiments

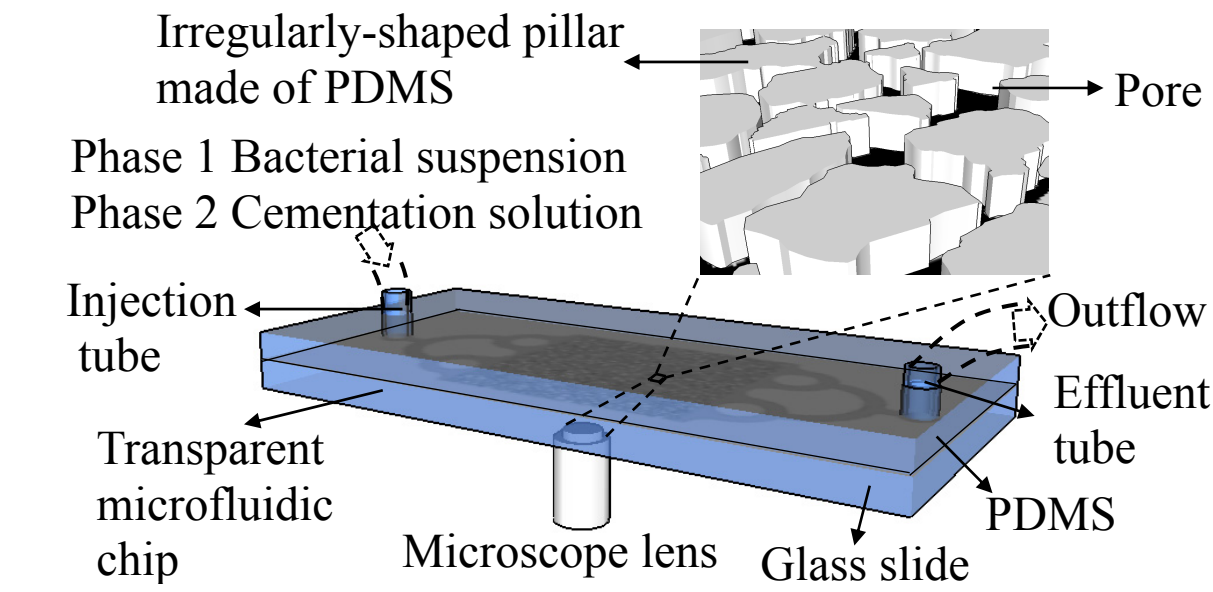

(a)

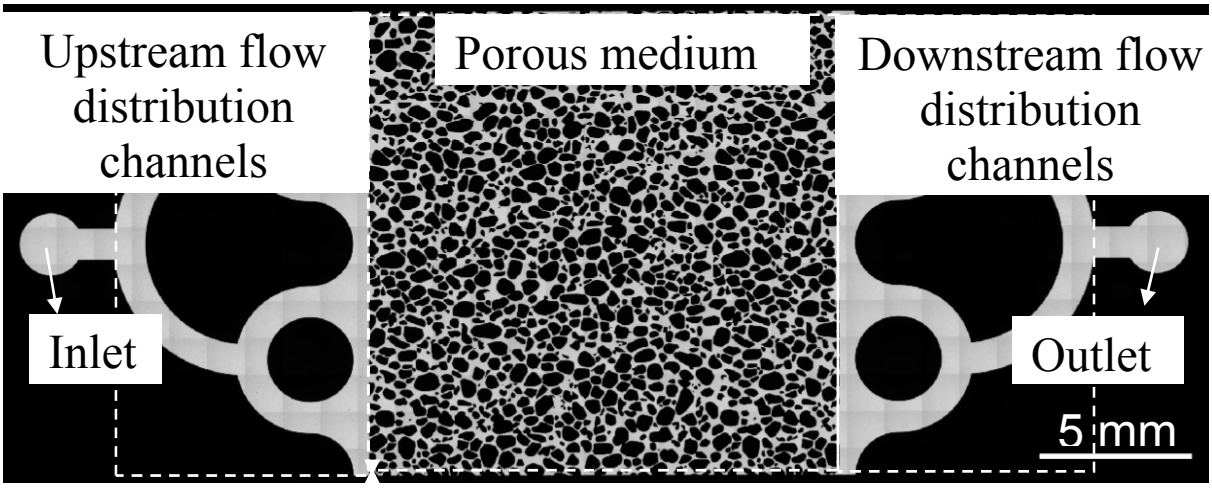

(b)

Fig. 3. (a) Schematic of setup for microfluidic chip experiments; (b) two-dimensional design of the microfluidic chip

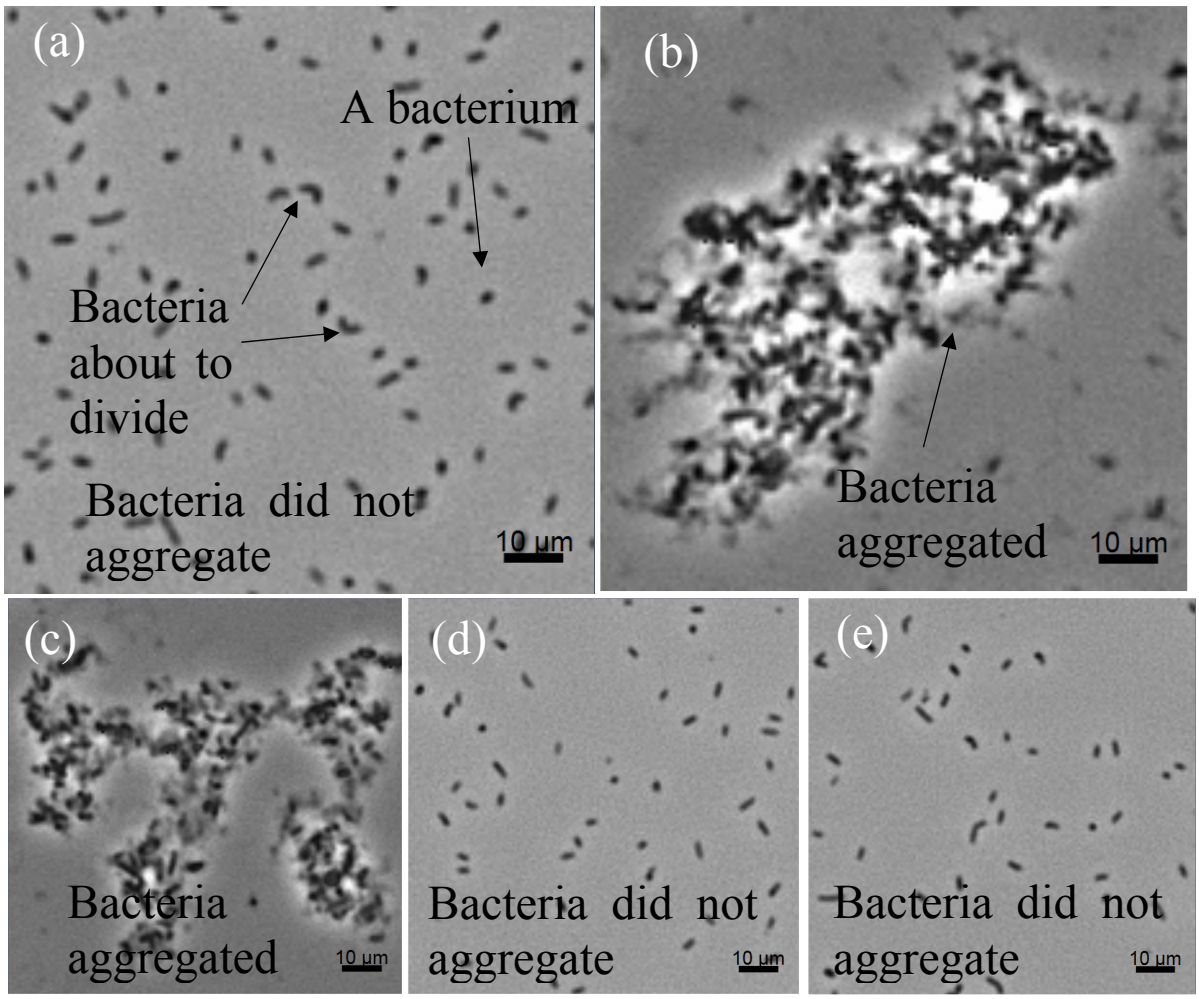

Fig. 4. Optical microscope images of (a) a bacterial suspension (OD_{600}=1.0), in which bacteria did not aggregate; (b) mixture of equal volumes of bacterial suspension (OD_{600}=1.0) and cementation solution (1.0 M $CaCl_2$, 1.5 M urea and 3 g/L nutrient broth), in which bacteria aggregated; (c) mixture of equal volumes of bacterial suspension (OD_{600}=1.0) and $CaCl_2$ solution (1.0 M), in which bacteria aggregated; (d) mixture of equal volumes of bacterial suspension (OD_{600}=1.0) and urea solution (1.5 M), in which bacteria did not aggregate; and (e) mixture of equal volumes of bacterial suspension (OD_{600}=1.0) and nutrient broth (3 g/L), in which bacteria did not aggregate

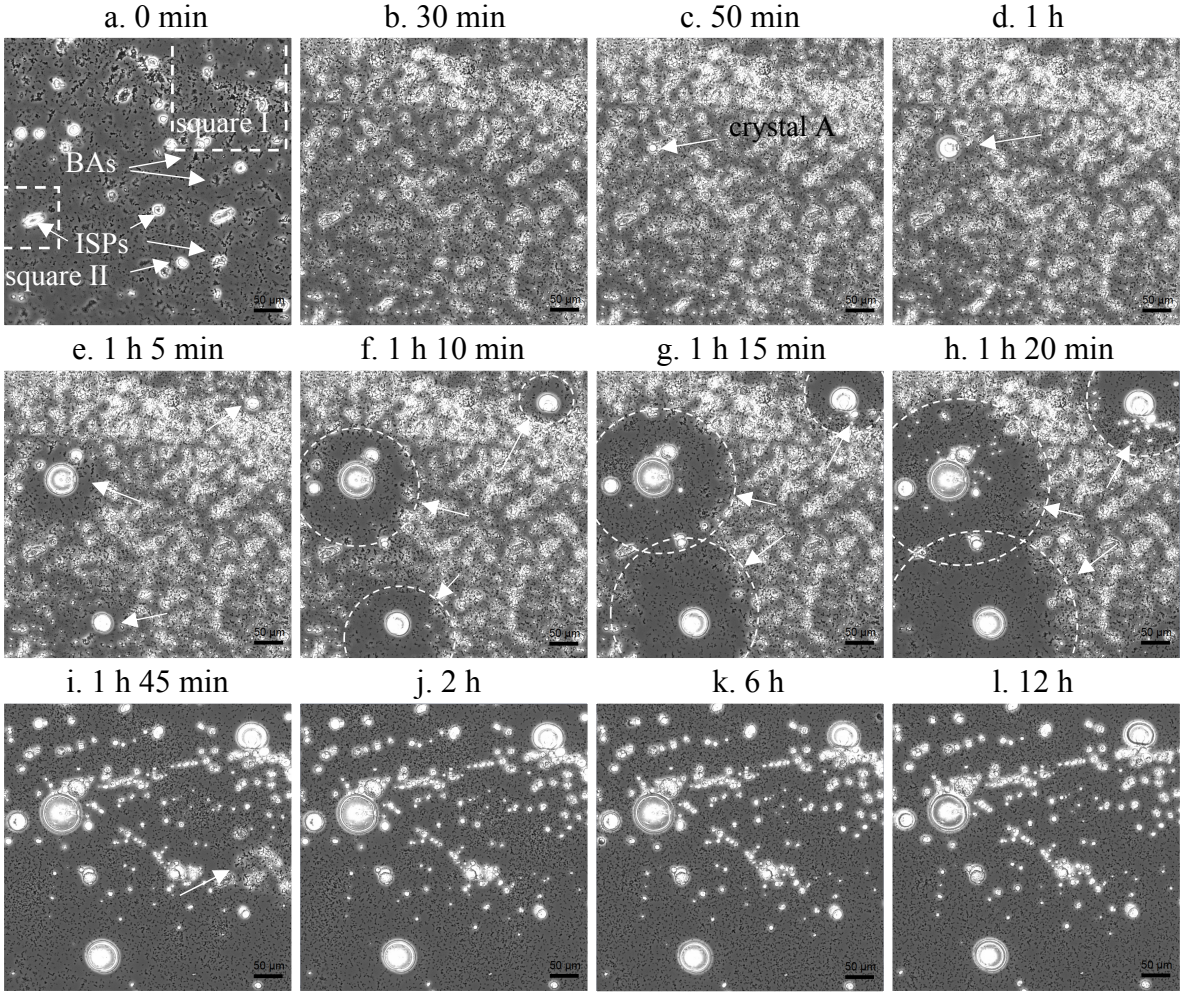

Fig. 5. Time-lapse microscope images of microscope glass slides containing the mixture of bacterial suspension and cementation solution. (a) at 0 min bacterial aggregates (BAs) and irregularly-shaped precipitates (ISP) formed; (b) by 30 mins more ISPs formed; (c) at 50 mins, crystal A formed (shown by the arrow) and ISPs became brighter compared with in image b; (d) crystal A became larger compared with in image c and ISPs surrounding crystal A dissolved; (e) at 1 h 5 min, new crystals formed (shown by arrows), crystal A continued growing and ISPs surrounding crystal A continued dissolving; (f-h) circular zones where ISPs dissolved became larger with time as shown by the arrows; (i) undissolved ISPs (shown by arrow); (j-l) only regularly-shaped crystals remained after 2 hours

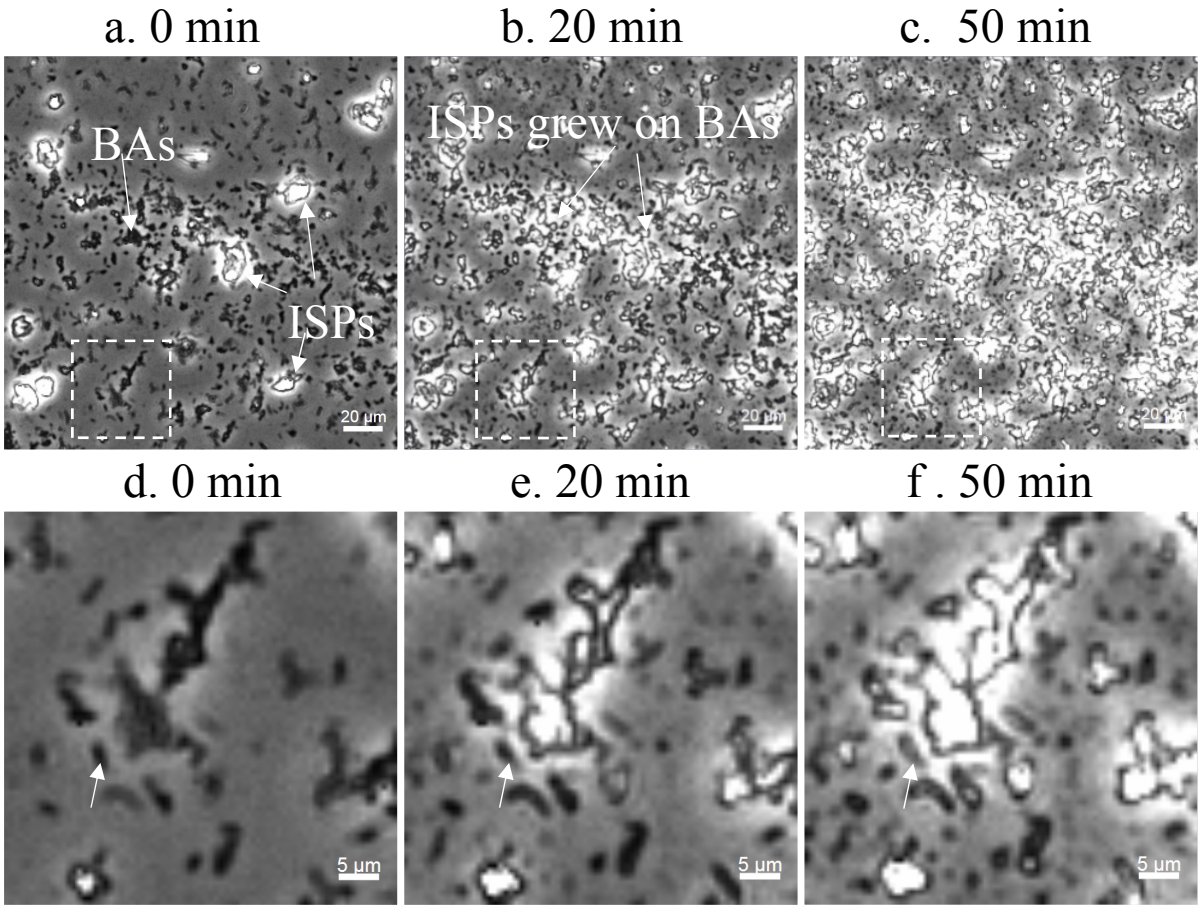

Fig. 6. Microscope images showing the precipitation of irregularly-shaped precipitates (ISPs) and the fixation of bacterial cells during the precipitation process. (a) at 0 min, bacterial aggregates (BAs) and irregularly-shaped precipitates (ISPs) formed; (b and c) ISPs formed on bacterial aggregates; (d and e) a bacterial cell shown by arrow; (f) at 50 mins, ISPs grew on the bacterial cell shown by arrow

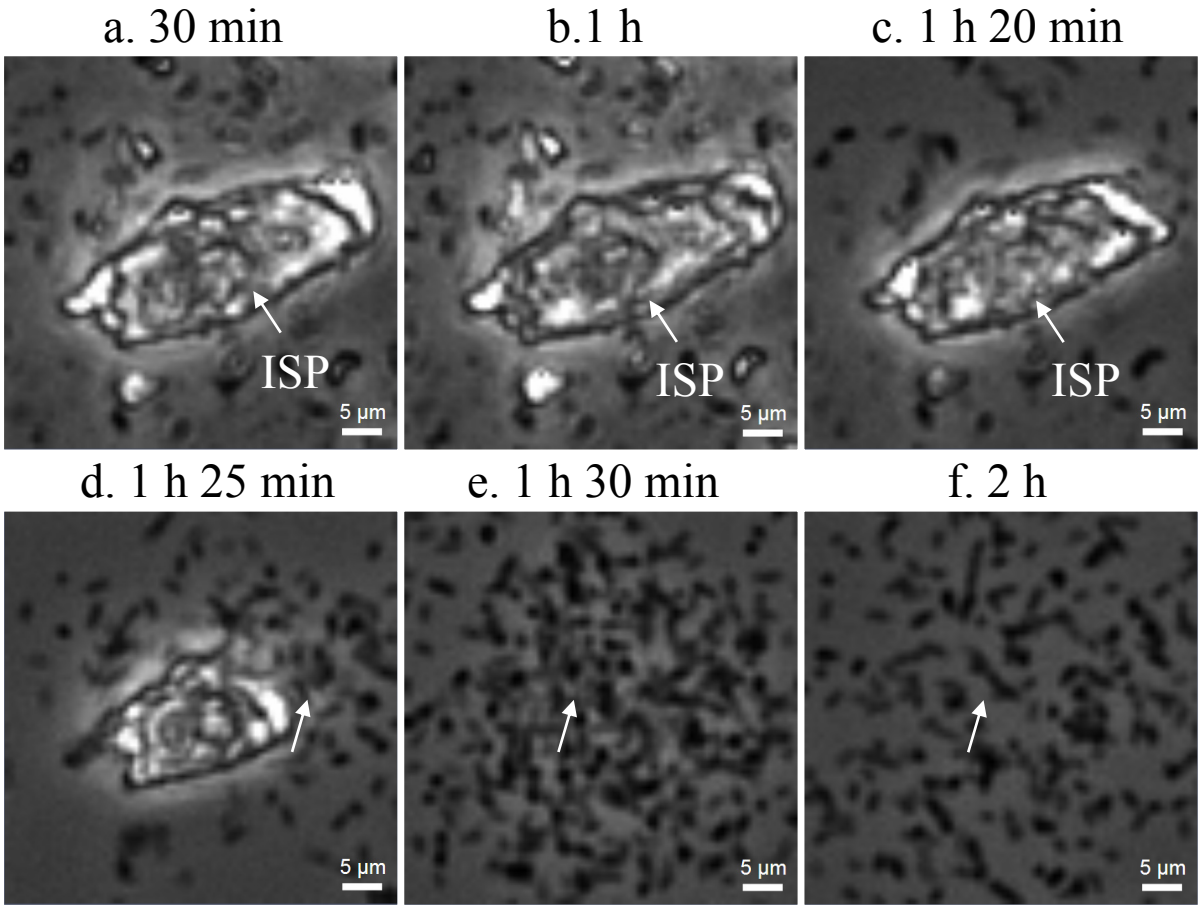

Fig. 7. The dissolution of an irregularly-shaped precipitate (ISP) and the movement of bacterial cells after the dissolution of the ISP. (a-c) irregularly-shaped precipitate (ISP); (d) by 1 h 25 min, half of the ISP dissolved with bacteria being released (indicated by arrow); (e) by 1 h 30 min, the whole ISP dissolved and bacteria released (indicated by arrow); (f) by 2 h, bacteria spread out (indicated by arrow)

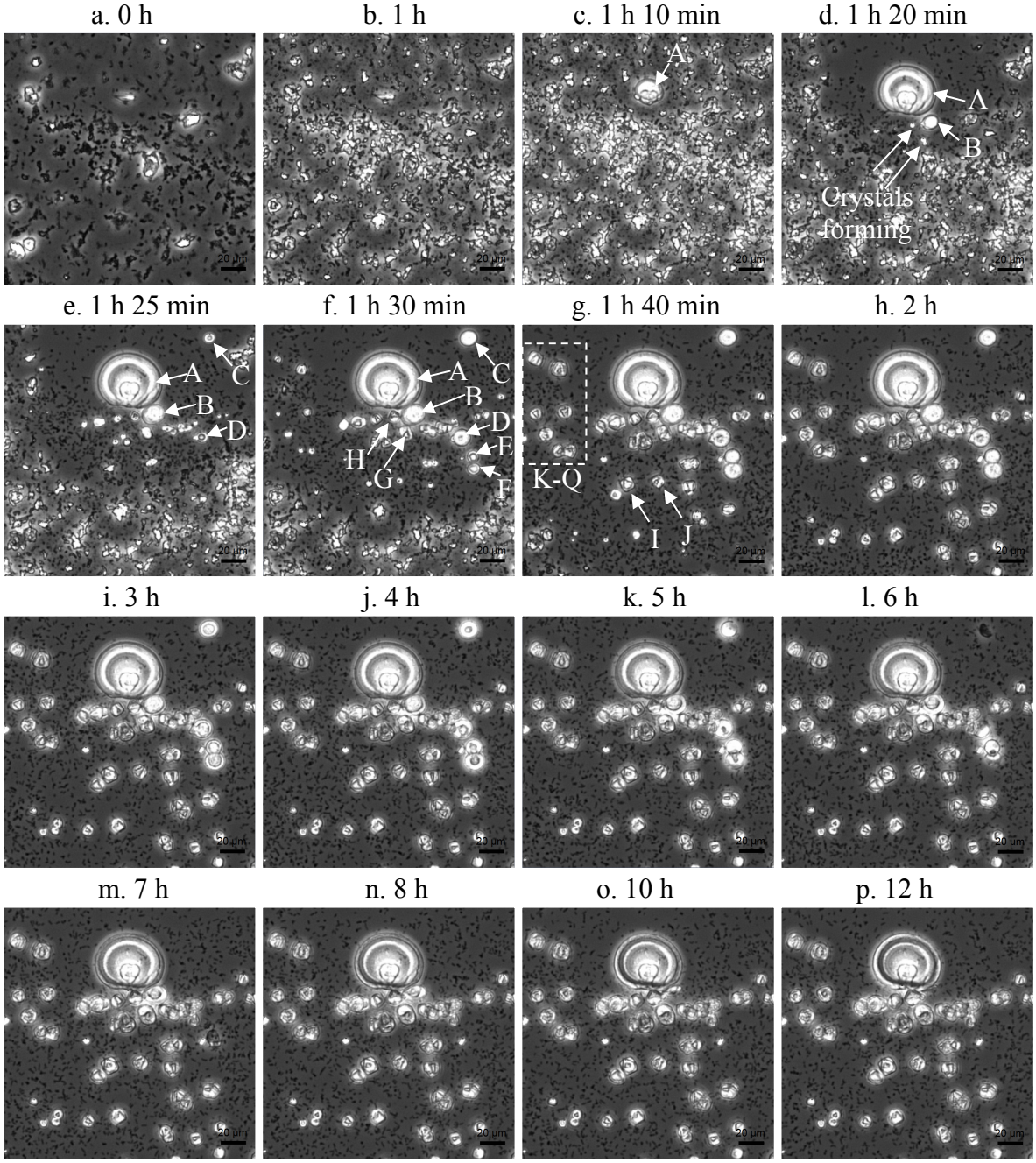

Fig. 8. Microscope images showing the dissolution of spherical $CaCO_3$ crystals while rhombohedral $CaCO_3$ crystals continued to be stable. (a-c) growth of irregularly-shaped $CaCO_3$ precipitates; (c-h) growth of spherical $CaCO_3$ crystals and rhombohedral $CaCO_3$ crystals at the expense of the dissolution of irregularly-shaped $CaCO_3$ precipitates; (i-p) rhombohedral $CaCO_3$ crystals stayed stable, whereas spherical $CaCO_3$ crystals dissolved. Scale bar 20 µm

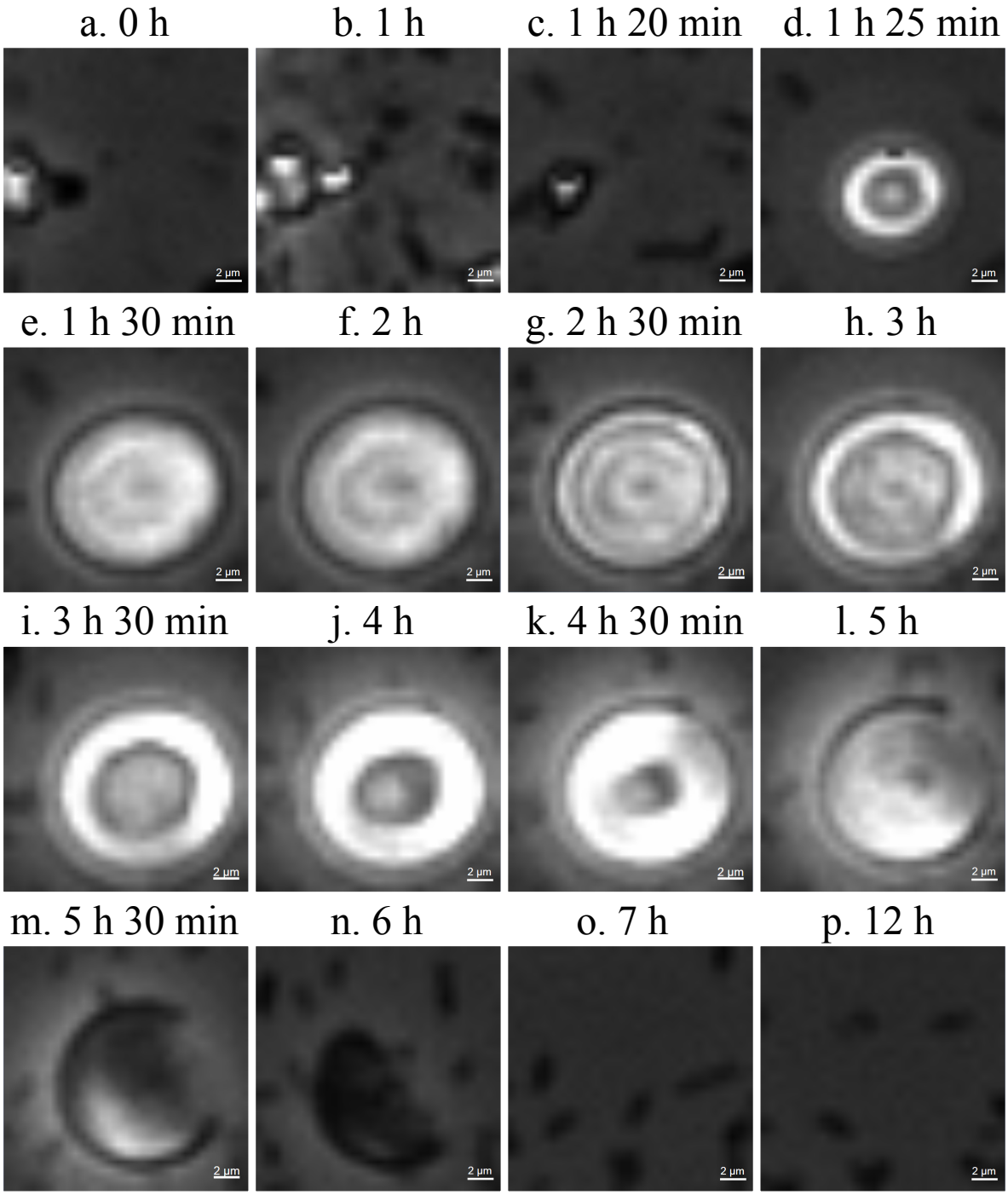

Fig. 9. Microscope images showing the growth and dissolution of a spherical $CaCO_3$ crystal. (a-c) events preceding the formation of the crystal; (d-f) growth of the crystal; (g-n) dissolution of the crystal; (o-p) events after the dissolution of the crystal. Scale bar 2 µm

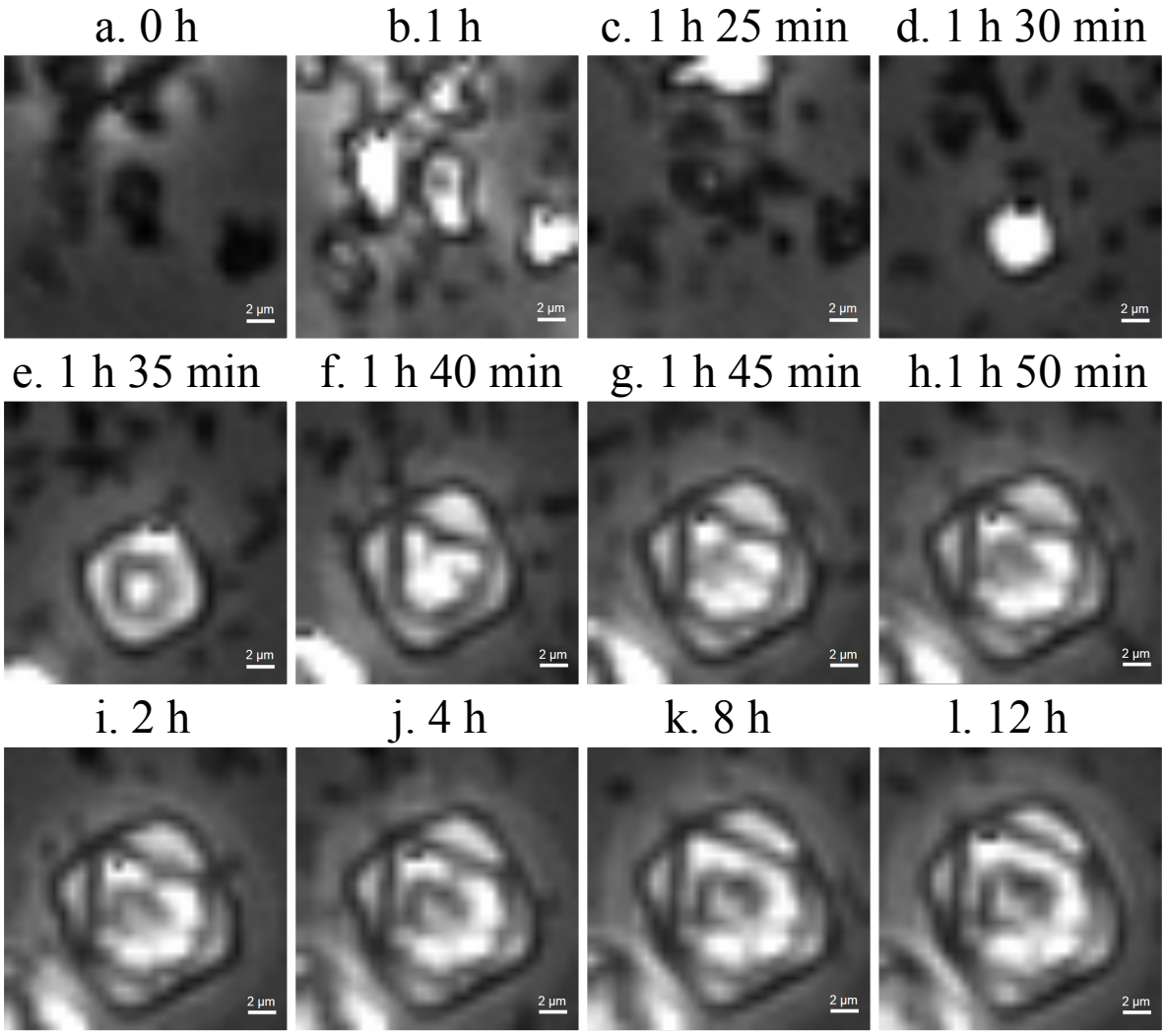

Fig. 10. Microscope images showing the growth of a rhombohedral $CaCO_3$ crystal. (a-c) events preceding the formation of the crystal; (d-l) crystal formation and growth. Scale bar 2 µm

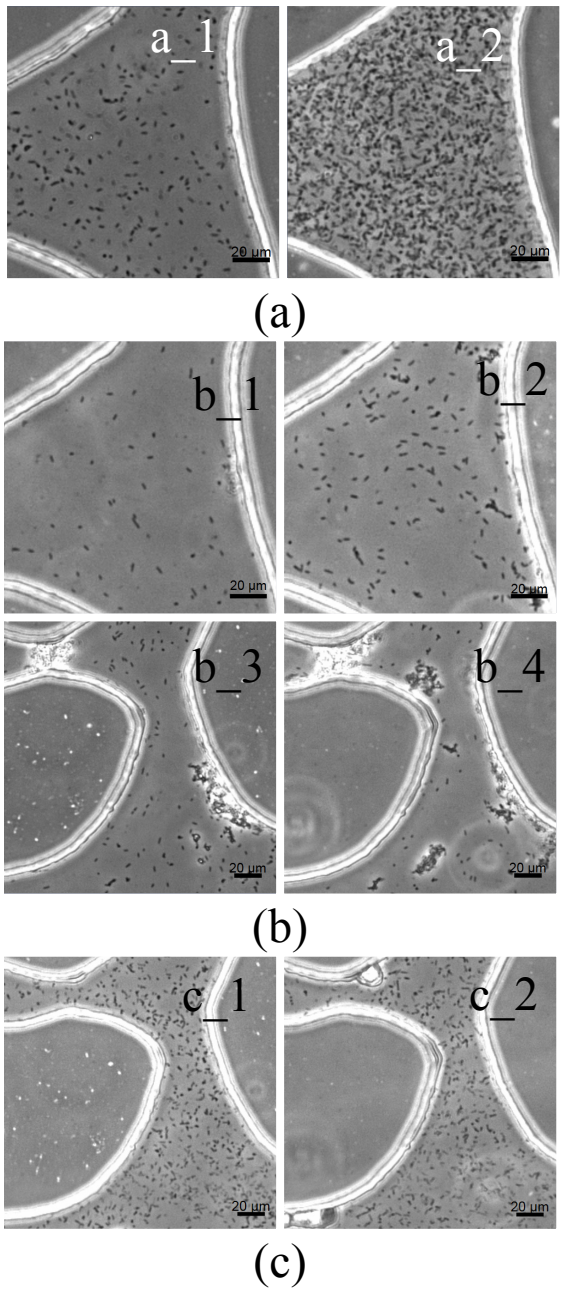

Fig. 11. (a) Microscope images of bacteria inside the central pore of the microfludic chip after the injection of bacterial suspension (a_1) and after bacterial settling (a_2); (b) Microscope images of bacteria inside two central pores of the microfludic chip after the injection of cementation solution at injection flow rates of 0.5 ml per hour (b_1, b_3) and 0.05 ml per hour (b_2, b_4); (c) Microscope images of bacteria inside the central pore at 24 hours after cementation solution injection at injection flow rates of 0.5 ml per hour (c_1) and 0.05 ml per hour (c_2)

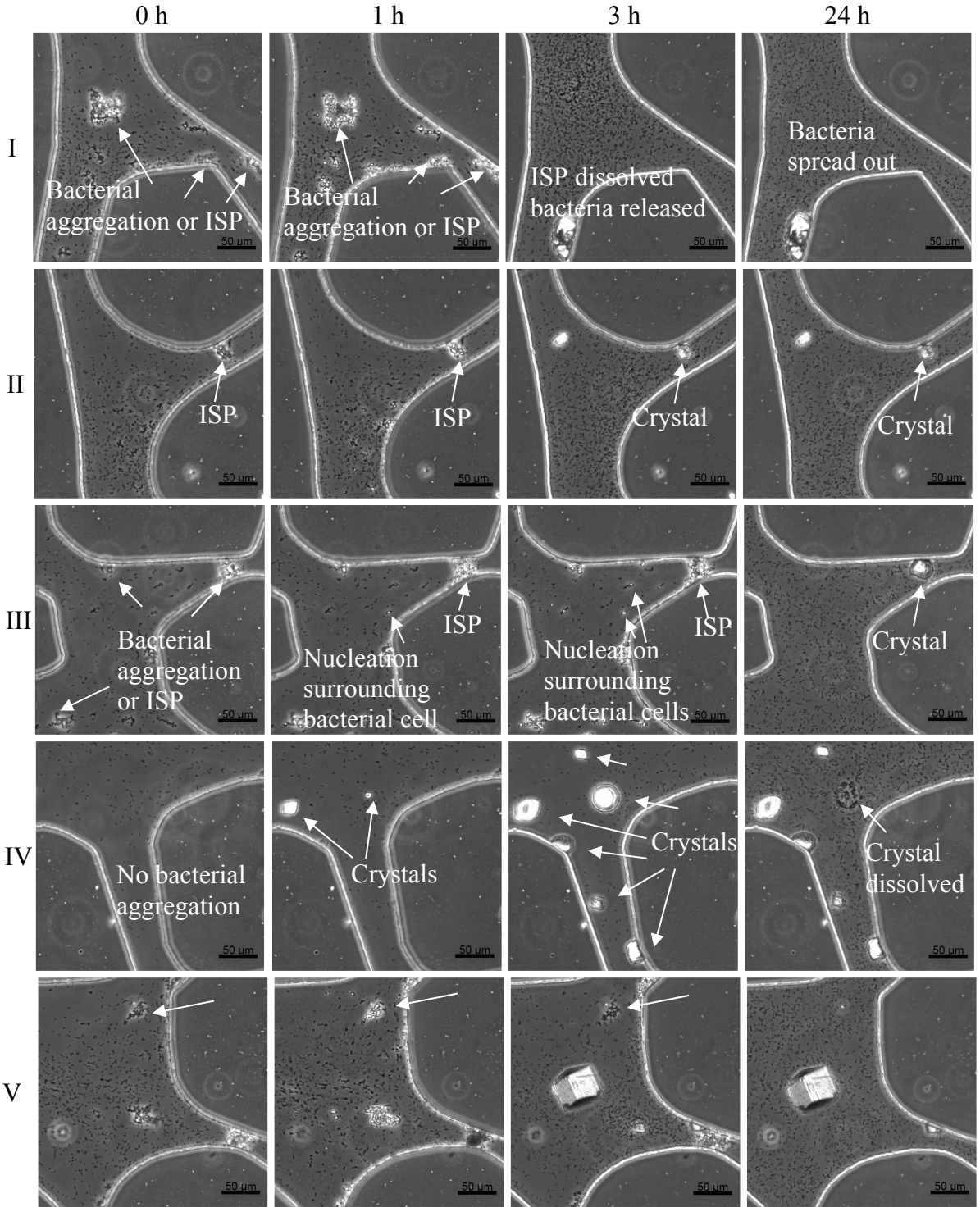

Fig. 12. Microscope images of five pores in the microfluidic chip (protocol 2) at 0, 1, 3 and 24 hours after the first injection of cementation solution

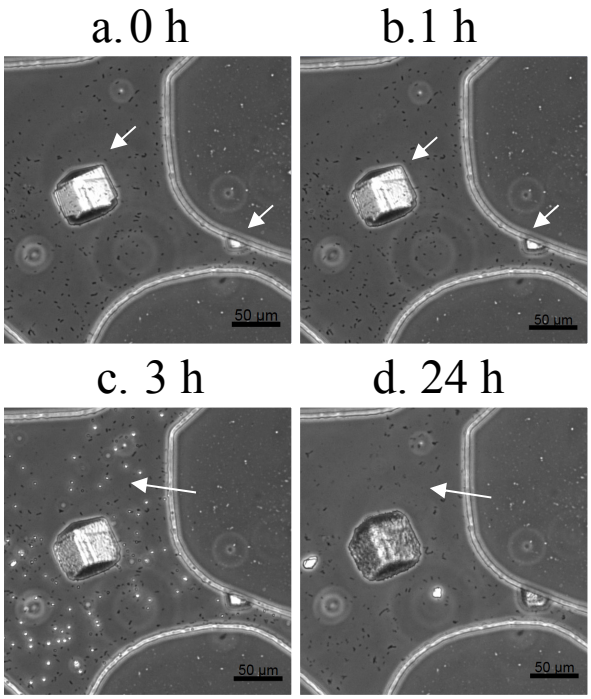

Fig. 13. Microscope images of pore V in the microfluidic chip (protocol 2) at 0, 1, 3 and 24 hours after the second injection of cementation solution. (a-b) 0-1 h, two crystals formed from the first injection of cementation solution (shown by arrows); (c) by 3 hrs, relatively small crystals formed (indicated by arrow); (d) by 24 hrs, relatively small crystals dissolved (indicated by arrow), whereas relatively large crystals remained

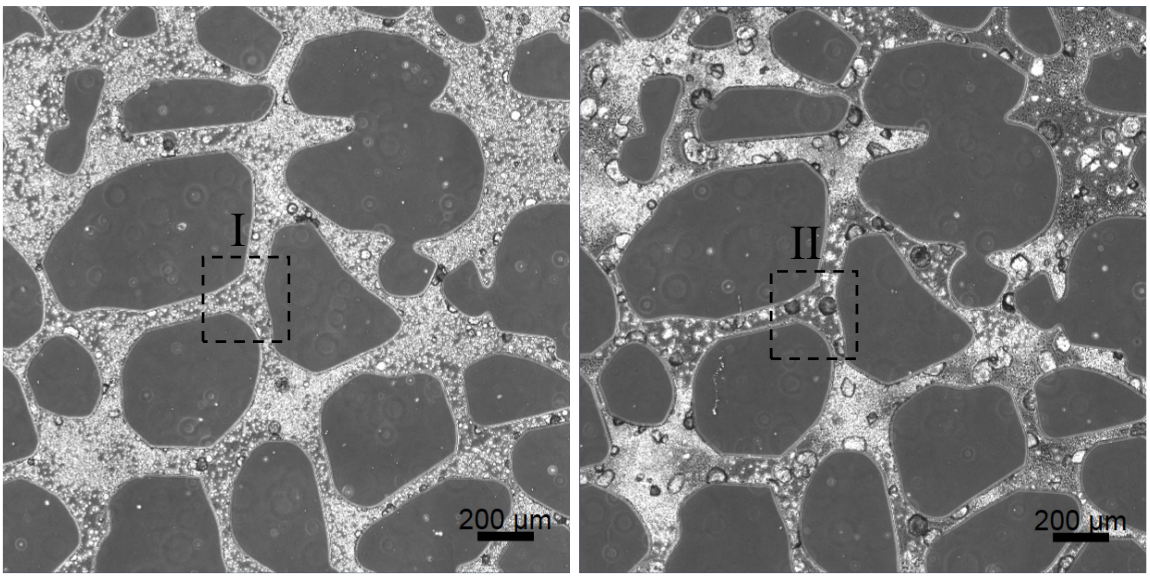

(a)

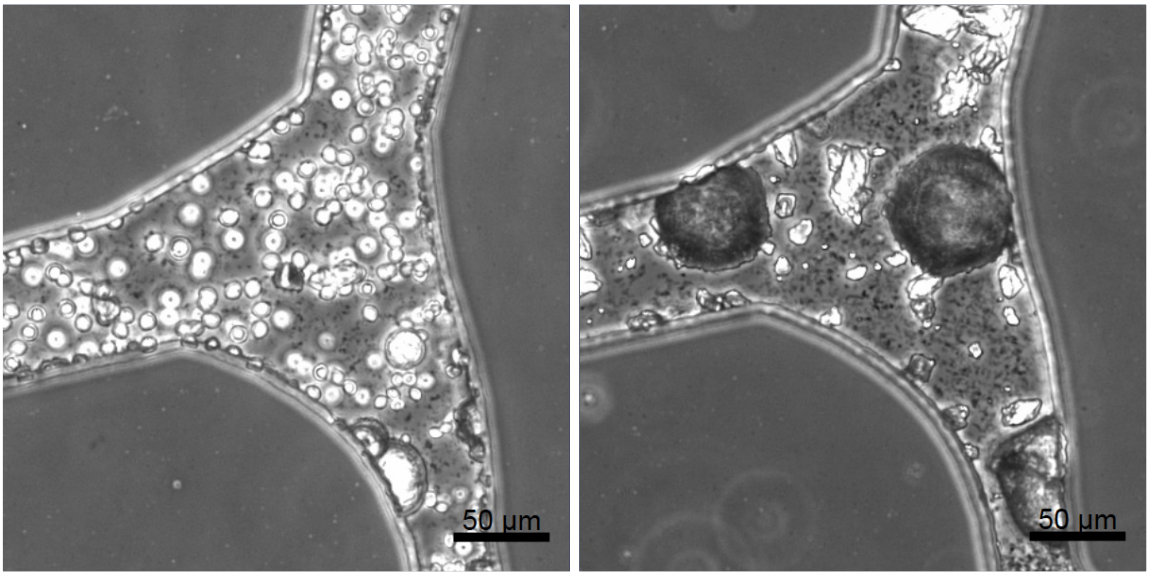

(b)

Fig. 14. (a) Microscope images of middle 3 mm by 3 mm squares of microfluidic chips at one day after the completion of the twelfth cementation solution injection at 3-5 hours interval (left image, protocol 3_1) and 23-25 hours interval (right image, protocol 3_2); (b) Magnified images of square I (left image) and square II (right image)